

CT Radiomics Combined With Clinicopathological Features to Predict Invasive Mucinous Adenocarcinoma in Patients With Lung Adenocarcinoma

Technology in Cancer Research & Treatment
Volume 22: 1-10
© The Author(s) 2023
Article reuse guidelines:
sagepub.com/journals-permissions
DOI: 10.1177/15330338231174306
journals.sagepub.com/home/tct



Junjie Zhang, MD^{1,2,*}, Ligang Hao, MD^{3,*} , Min Li, MD¹, Qian Xu, MD¹, and Gaofeng Shi, MD¹

Abstract

Objective: This study aimed to develop and validate predictive models using clinical parameters, radiomic features, and a combination of both for invasive mucinous adenocarcinoma (IMA) of the lung in patients with lung adenocarcinoma. **Method:** A total of 173 and 391 patients with IMA and non-IMA, respectively, were retrospectively analyzed from January 2017 to September 2022 in our hospital. Propensity Score Matching was used to match the 2 groups of patients. A total of 1037 radiomic features were extracted from contrast-enhanced computed tomography (CT). The patients were randomly divided into training and test groups at a ratio of 7:3. The least absolute shrinkage and selection operator algorithm was used for radiomic feature selection. Three radiomics prediction models were applied: logistic regression (logistic), support vector machine (SVM), and decision tree. The best-performing model was adopted, and the radiomics score (Radscore) was then computed. A clinical model was developed using logistic regression. Finally, a combined model was established based on a clinical model and a radiomics model. The area under the receiver operating characteristic (ROC) curve (AUC) and decision curve analysis were used to evaluate the predictive value of the developed models. **Results:** Both clinical and radiomics models established using the logistic method showed the best performance. The Delong test revealed that the combined model was superior to the clinical and radiomics models ($P = .018$ and $.020$, respectively). The ROC-AUC (also decision curve analysis) of the combined model was 0.840 and 0.850 in the training and testing groups, respectively, which showed good predictive performance for IMA. The Brier scores for the combined model were 0.161 and 0.154 in the training and testing groups, respectively. **Conclusion:** The combined model incorporating radiomic CT features and clinical predictors may have the potential to predict IMA in patients with lung cancer.

Keywords

radiomics, contrast-enhanced CT, predictive model, invasive mucinous adenocarcinoma, lung adenocarcinoma

Abbreviations

AUC, area under the curve; CT, computed tomography; DCA, Decision curve analysis; GLCM, Gray Level Co-occurrence Matrix; GLDM, Gray Level Dependence Matrix; GLRLM, Gray Level Run Length Matrix; GLSZM, Gray Level Size Zone Matrix; ICC, inter-class correlation coefficients; IMA, invasive mucinous adenocarcinoma; LASSO, least absolute shrinkage and selection operator; MPR, multiplanar reconstruction; NGTDM, Neighboring Gray Tone Difference Matrix; ROC, receiver operating characteristic; SVM, support vector machine.

Received: October 10, 2022; Revised: March 13, 2023; Accepted: April 3, 2023.

¹ Department of Computed Tomography and Magnetic Resonance, The Fourth Hospital of Hebei Medical University, Shijiazhuang, He Bei, China

² Department of CT & MR, The First Hospital of Xing Tai, Xing Tai, He Bei, China

³ Department of Thoracic Surgery Xing Tai People's Hospital, Xing Tai, He Bei, China

*Ligang Hao and Junjie Zhang contributed equally to this manuscript.

Corresponding Author:

Qian Xu, Department of Computed Tomography and Magnetic Resonance, Hebei Medical University Fourth Affiliated Hospital, 12 Jiankang Road, Shijiazhuang, 050011, Hebei, China.

Emails: xuqianhbydsy@163.com; nihaozhangjunjie@126.com



Creative Commons Non Commercial CC BY-NC: This article is distributed under the terms of the Creative Commons Attribution-NonCommercial 4.0 License (<https://creativecommons.org/licenses/by-nc/4.0/>) which permits non-commercial use, reproduction and distribution of the work without further permission provided the original work is attributed as specified on the SAGE and Open Access page (<https://us.sagepub.com/en-us/nam/open-access-at-sage>).

Introduction

Lung cancer is the leading cause of cancer-related deaths and the second most commonly diagnosed cancer worldwide.¹ Nonsmall cell lung cancer (NSCLC) accounts for almost 85% of all primary lung cancers, among which adenocarcinoma is the most common pathological subtype.^{2,3} Primary invasive mucinous adenocarcinoma (IMA) is a rare subtype of lung adenocarcinoma. It accounts for only 2% to 10% of lung adenocarcinoma.^{4,5} Due to its unique pathological, radiological, and prognostic characteristics, it has been separated from other adenocarcinomas and previously classified as nonmucinous bronchoalveolar carcinoma, according to the International Association for the Study of Lung Cancer/American Thoracic Society/European Respiratory Society classification system for lung adenocarcinoma published in 2011. In 2015, the World Health Organization (WHO) also classified IMA as an invasive adenocarcinoma subtype.⁶

Molecular biological differences between IMA and invasive nonmucinous adenocarcinoma affect the prognosis and treatment options of patients.⁷⁻⁹ Previous studies have shown that anaplastic lymphoma kinase (ALK), Kirsten rat sarcoma viral oncogene (KRAS), and co-occurring oncogenic mutations were observed more commonly in patients with IMA than in those with invasive nonmucinous adenocarcinoma.¹⁰ Previous studies revealed that the frequency of epidermal growth factor receptor (EGFR) (72.0% vs 40.0% vs 23.1%, $P = .002$) and ALK (undetected vs 20.0% vs 26.9%, $P = .015$) alterations showed a trend of gradual decrease and increase from non-IMA to mixed-IMA to pure-IMA, respectively.¹¹ Another study showed that KRAS mutations were more common in IMA than in other adenocarcinomas (14%-86% in IMA vs 1.5%-17% in non-IMA).¹¹⁻¹⁶ These driver mutations influenced the choice of clinical drug treatment options. In addition, patients with IMA have significantly different outcomes compared to those with other types of adenocarcinoma.⁹ However, nearly 80% of NSCLC patients, including patients with IMA, are diagnosed at an advanced stage and have no opportunity to undergo radical surgical treatment.¹⁷ In these patients, the common methods to obtain these tissue specimens include tissue or liquid biopsy. Sometimes, these specimens cannot represent the entire tumor, as the tumor tissue varies with respect to time and space. Therefore, to evaluate the prognosis of patients accurately and guide precision treatment, it is necessary to find a Supplemental Material to predict IMA.

Computed tomography (CT) is widely used for tumor detection, staging, and therapeutic response monitoring in clinical practice.^{18,19} However, the noninvasive imaging diagnostic information provided by preoperative CT images is still limited and cannot differentiate IMA from non-IMA. Radiomics proposes a method to extract quantitative and high-throughput data from medical images, which reflect the underlying pathophysiology and reveal information on tumor phenotypes.²⁰ In the past decade, radiomics, as an alternative to biopsies, achieved a favorable performance in predicting malignancy risk, gene expression pattern, and the tumor microenvironment in lung cancer and in quick diagnosis during the COVID-19 pandemic.²¹⁻²⁴ Based on these former explorations, to better satisfy the need for precise evaluation of

pathology, radiomics features were used to develop a model to predict the IMA of the lung.

Materials and Methods

This study was performed following the Helsinki Declaration and approved by the Ethics Committee of our hospital. This study was performed following the Helsinki Declaration and approved by the Ethics Committee of our hospital (Ethics Committee of Hebei Medical University Fourth Affiliated Hospital, reference number: 2022KS017, data 2022.6.27). Ethical approval was obtained from our hospital, and waivers of consent were granted to the study subjects.

Patients' Selection

We retrospectively analyzed patients diagnosed with lung adenocarcinoma between January 2017 and September 2022 in our hospital. The inclusion criteria were as follows: (1) patients with IMA and non-IMA diagnosed by needle biopsy or surgical pathology, with imaging showing a peripheral lung cancer; (2) patients with complete clinical and pathological data, which can provide analyzable plain and enhanced thin-slice CT image data (1 or 1.25 mm/slice); and (3) availability of CT images taken within 2 weeks before pathological diagnosis. The exclusion criteria for patients were as follows: (1) patients on anti-tumor therapy (including radiotherapy, chemotherapy, chemoradiotherapy, or molecular targeted therapy) prior to CT examination and pathological diagnosis; (2) pathologically mixed mucinous adenocarcinoma (ie, nonmucinous adenocarcinoma component $\geq 10\%$) or imaging manifestations of pneumonic mucinous adenocarcinoma; (3) too small size of the primary lesion (the largest diameter of the lesion < 0.5 cm) to be segmented; and (4) patients with other types of cancer or with incomplete clinical and imaging data. All patients with IMA matching the inclusion criteria were enrolled from January 2017 to September 2022 at our hospital. In addition, 391 patients with non-IMA matching the inclusion criteria were randomly selected between January 2017 and September 2022 in our hospital. Propensity Score Matching (PSM) was used to match the 2 groups of patients. A previous study revealed no significant difference in age between patients with IMA and non-IMA.¹¹ However, patients with non-IMA developed metastasis much more easily. To eliminate the confounding factors, the matching factors included age and tumor diameter, and the matching ratio was 1:1.

CT Image Acquisition

For all patients, contrast-enhanced chest CT scans were performed using one of the following multidetector row scanners: Somatom Sensation 64, Definition Flash (Siemens Medical Solutions, Forchheim, Germany), and Discovery CT 750 HD (Revolution; GE Medical Systems, Milwaukee, Wisconsin, USA). Before scanning, the patients were trained to breathe and hold their breath at the end of inspiration to scan. The range included the thoracic inlet to

the base of the lung. Scanning parameters were as follows: (1) Siemens SOMATOM Definition Flash CT: tube voltage 120 kV, tube current using automatic mAs, a reconstruction layer thickness of 1 mm, matrix 512×512 , pitch 1.2; (2) GE Revolution CT: tube voltage 120 kV, tube current 200 mAs, a reconstruction layer thickness of 1.25 mm, matrix 512×512 , and pitch 1.2. The reconstruction algorithm adopted was a lung algorithm. After the plain scan was completed, a bolus dose of (70-90 mL) nonionic contrast agent iohexol or ioversol (300 mg-I/mL) was injected through the cubital vein using a high-pressure syringe at a flow rate of 3 mL/s. Arterial and venous phase dual-phase enhanced scans were performed 30 and 90 s after the contrast agent, respectively. Other parameters were the same as those of the plain scans. After scanning, the raw data were uploaded to a postprocessing workstation for multiplanar reconstruction (MPR).

Image feature analysis was performed by 2 board-certified thoracic radiologists (with 6 and 12 years of experience in chest CT imaging, respectively) who were blinded to clinical and histological findings. All CT image features were independently recorded by 2 radiologists, and any discrepancies in assessments were consistently resolved. The mediastinal window (window width 400 HU; window level 40 HU) and lung window (window width 1200 HU; window level -600 HU) were set. The CT image features recorded in the image analysis are as follows: (1) primary tumor location (left and right lungs, upper, middle, and lower lobes); (2) adjacent to pleura (the minimum distance between the lesion and the pleura is < 1 cm); (3) tumor size (maximum diameter), type (ground glass density, partially solid, and solid), average CT value (unenhanced scan, arterial phase, and venous phase), ΔCT_A value (the difference between the CT value of the arterial phase and the CT value of the plain scan), ΔCT_V value (the difference of the CT value of the venous phase and the CT value of the plain scan), shape (round or quasi-round, irregular), and edge (lobular, blur); (4) internal features of the tumor (calcification, necrosis, cyst, air bronchus sign, etc); (5) external features of the tumor (thickening of adjacent bronchovascular bundles, pleural depression, and obstructive changes).

Segmentation, Feature Extraction, and Selection

CT images were imported into an open-source software ITK-SNAP (version 3.6.0, <http://www.itksnap.org>) and read under lung window (width 1200/-600 HU) and mediastinal window (width 400/40 HU) settings. The primary lesions of patients with adenocarcinomas were selected for tumor segmentation after image acquisition. A radiologist without knowledge of the clinical data manually delineated the regions of interest (ROI) layer by layer. The tumor ROI encompassed the entire lesion as much as possible, including the bronchi, blood vessels, and vacuoles within the nodules, and excluded the normal lung tissue. Tumor segmentation was performed on 50 patients randomly selected from the entire cohort for independent segmentation to assess intraclass agreement one month later. Another radiologist repeated the independent segmentation of the selected 50 patients and evaluated the

interclass agreement. Intra- and interclass correlation coefficients (ICCs) were used to assess the intraobserver and interobserver reproducibility of feature extraction.

Pyradiomics was used to extract the radiomics features.²⁵ A total of 1037 features were extracted, including 17 classes of histogram, 14 classes of form factor, 24 classes of Gray Level Co-occurrence Matrix (GLCM), 16 classes of Gray Level Run Length Matrix (GLRLM), 16 classes of Gray Level Size Zone Matrix (GLSZM), 5 classes of Neighboring Gray Tone Difference Matrix (NGTDM), and 14 classes of Gray Level Dependence Matrix (GLDM).

To reduce the dimensionality of radiomic features to the number of events, we performed 3 sequential steps for radiomic feature selection. First, we evaluated the interobserver agreement of radiomic features and selected features showing $ICC > 0.75$. Next, we chose radiomic features that showed statistical significance between the IMA and non-IMA groups. Finally, the least absolute shrinkage and selection operator (LASSO) logistic regression model was used to select the most useful predictive features of radiomics for IMA in the training group. Five-fold cross-validation was performed 100 times to avoid overfitting.

Model Development

Three radiomics prediction models: logistic regression (logistic), support vector machine (SVM), and decision tree were applied. The receiver operating characteristic (ROC) curve was used to evaluate the performance of the 3-machine-learning model. The best-performing model was adopted, and the radiomics score (Radscore) was then computed.

At the same time, we constructed a model based on clinical and CT features for multivariate logistic regression analysis. The clinical features included sex, age, and smoking status. The CT features have been illustrated above.

Finally, 3 models, namely the clinical model, the radiomics model, and a combination of clinical and radiomics models, were compared statistically to identify the model with higher predictability.

Statistical Analysis

All statistical analyses were performed using R version 3.6.3 and Python version 3.7. The patients were randomly divided into training and test groups at a ratio of 7:3. All radiomic features were subjected to Z-score normalization. Baseline data were analyzed by univariate analysis using Python statistical model 0.11.1. The chi-square test was used for categorical variables, and the *t*-test or Mann-Whitney *U*-test was used for continuous variables. Factors with statistical differences ($P < .05$) were included in the multivariate logistic regression analysis. Clinical and CT features with statistical differences ($P < .05$) in the multivariate analysis results were selected to construct the clinical diagnostic model.

The main evaluation indicators were the area under the ROC curve (AUC), accuracy, sensitivity, specificity, positive predictive value, and negative predictive value. Decision curve analysis (DCA) was used to calculate the clinical impact of the 3 models.

Results

Patient Characteristics

A total of 173 and 391 patients with IMA and non-IMA, respectively, were retrospectively analyzed. Finally, 173 patients with non-IMA were screened and matched with 173 patients with pulmonary IMA. The patients were randomly divided into training

and test groups at a ratio of 7:3. The training group included 242 patients (125 and 117 patients with IMA and non-IMA, respectively). The testing group included 104 patients (56 and 48 patients with IMA and non-IMA, respectively). The characteristics of the patients in the training and testing cohorts are shown in detail in Table 1. The average age was 61 years (range was 18-83 years). There were no significant differences in the clinical

Table 1. Clinical Characteristics of Patients.

| Characters | Training cohort | | | Testing cohort | | |
|-------------------------------|-------------------------|-------------------------|----------|-------------------------|-------------------------|----------|
| | NIMA | IMA | <i>P</i> | NIMA | IMA | <i>P</i> |
| Smoking | | | | | | |
| No | 64 | 75 | .405 | 38 | 33 | .922 |
| Yes | 53 | 50 | | 18 | 15 | |
| Solid | | | | | | |
| No | 65 | 81 | .142 | 15 | 10 | .479 |
| Yes | 52 | 44 | | 41 | 38 | |
| Lobul | | | | | | |
| No | 40 | 33 | .187 | 18 | 11 | .296 |
| Yes | 77 | 92 | | 38 | 37 | |
| Spicul | | | | | | |
| No | 72 | 74 | .710 | 30 | 31 | .256 |
| Yes | 45 | 51 | | 26 | 17 | |
| Cyst | | | | | | |
| No | 95 | 64 | <.001 | 43 | 23 | .002 |
| Yes | 22 | 61 | | 13 | 25 | |
| Necrosis | | | | | | |
| No | 86 | 117 | <.001 | 39 | 43 | .013 |
| Yes | 31 | 8 | | 17 | 5 | |
| Edge | | | | | | |
| No | 17 | 12 | .238 | 10 | 6 | .450 |
| Yes | 100 | 113 | | 46 | 42 | |
| VS | | | | | | |
| No | 93 | 83 | .022 | 52 | 29 | <.001 |
| Yes | 24 | 42 | | 4 | 19 | |
| BS | | | | | | |
| No | 105 | 106 | .250 | 51 | 39 | .143 |
| Yes | 12 | 19 | | 5 | 9 | |
| PLT | | | | | | |
| No | 45 | 108 | <.001 | 21 | 33 | .001 |
| Yes | 72 | 17 | | 35 | 15 | |
| BCS | | | | | | |
| No | 73 | 103 | <.001 | 33 | 40 | .007 |
| Yes | 44 | 22 | | 23 | 8 | |
| LL | | | | | | |
| No | 78 | 47 | <.001 | 36 | 17 | .003 |
| Yes | 39 | 78 | | 20 | 31 | |
| Gender | | | | | | |
| Male | 62 | 62 | .642 | 22 | 16 | .530 |
| Female | 55 | 62 | | 34 | 32 | |
| ΔCT _v median [IQR] | 37.000 [10.000, 66.625] | 24.000 [12.000, 76.000] | <.001 | 32.000 [22.000, 51.000] | 25.000 [14.000, 46.000] | .018 |
| Diameter, median [IQR] | 2.300 [1.400, 3.600] | 2.200 [1.500, 3.500] | .795 | 2.400 [1.400, 3.300] | 2.300 [1.300, 3.500] | .855 |
| Age, median [IQR] | 60.000 [53.000, 67.000] | 61.000 [56.000, 67.000] | .697 | 62.000 [56.000, 68.000] | 64.000 [57.000, 67.000] | .802 |

Abbreviations: IMA, invasive mucinous adenocarcinoma; NIMA, noninvasive mucinous adenocarcinoma; Lobul, lobulation; Spicul, spiculation; Cyst, Cyst cavity; VS, vascular passage; BS, bronchus sign; PLT, pleural traction; BCS, bronchus cutoff sign; LL, lesion location in the lower lobe; ΔCT_v, venous CT value – plain CT value.

characteristics (age, smoking, and sex) between the IMA and non-IMA groups (Table 1). Pleural traction, necrosis, and bronchus cutoff signs were more common in patients with non-IMA ($P < .05$, Table 1). Vascular passage, cystic cavity, early stage, and lower lobe lesion were more common in the IMA group ($P < .05$, Table 1). The ΔCT_V of IMA was significantly lower than that of non-IMA ($P < .05$, Table 1). A total of 16 patients with IMA underwent preoperative biopsy, of which 7 (43.750%) could not be identified as having mucinous adenocarcinoma and were only diagnosed with adenocarcinoma.

Feature Selection and Clinical Model Construction

Multivariate analysis showed that there were significant differences between mucinous adenocarcinoma and nonmucinous

Table 2. Multivariate Analysis to Identify Significant Factors for IMA.

| Predictors | <i>P</i> | OR | Lower | Upper |
|---------------|----------|-------|-------|-------|
| ΔCT_V | 0.0 | 0.185 | 0.087 | 0.37 |
| Cyst | 0.0 | 2.862 | 1.704 | 4.873 |
| VS | 0.006 | 2.241 | 1.268 | 4.04 |
| PLT | 0.013 | 0.533 | 0.324 | 0.872 |
| LL | 0.0 | 3.553 | 2.171 | 5.9 |

Abbreviations: Cyst, Cyst cavity; VS, vascular passage; PLT, pleural traction; LL, lesion location in the lower lobe; ΔCT_V , venous CT value -- plain CT value; OR, odds ratio.

adenocarcinoma in the cystic cavity, vascular passage bronchial truncation, lesion location in the lower lobe, pleural traction, and ΔCT_V (venous CT value – plain CT value). A clinical prediction model was established using logistic regression based on 5 features. The AUC values of the clinical models for predicting IMA were 0.780 and 0.770 in the training and testing cohorts, respectively. See Tables 2 and 3 for details.

Radiomics Feature Selection and Model Construction

To eliminate redundant features, 612 features that showed no significant difference between IMA and non-IMA and 411 features with ICC values < 0.75 were excluded. After screening out the redundant features by LASSO with the value of λ on the minimum standard and 1-standard error were 0.052 and 0.083,

Table 3. Diagnostic Performance of Prediction Models.

| Model | Training cohort | | | Testing cohort | | |
|----------|-----------------|-------|-------|----------------|-------|-------|
| | AUC | SEN | SPE | AUC | SEN | SPE |
| RADS | 0.720 | 0.664 | 0.667 | 0.770 | 0.771 | 0.750 |
| Clinical | 0.780 | 0.656 | 0.778 | 0.770 | 0.625 | 0.804 |
| Comb | 0.840 | 0.856 | 0.718 | 0.850 | 0.771 | 0.804 |

Abbreviations: AUC, area under the curve; SEN, sensitivity; SPE, specificity; Radiomics, radiomics model; Clinical, clinical model; Comb, combined model.

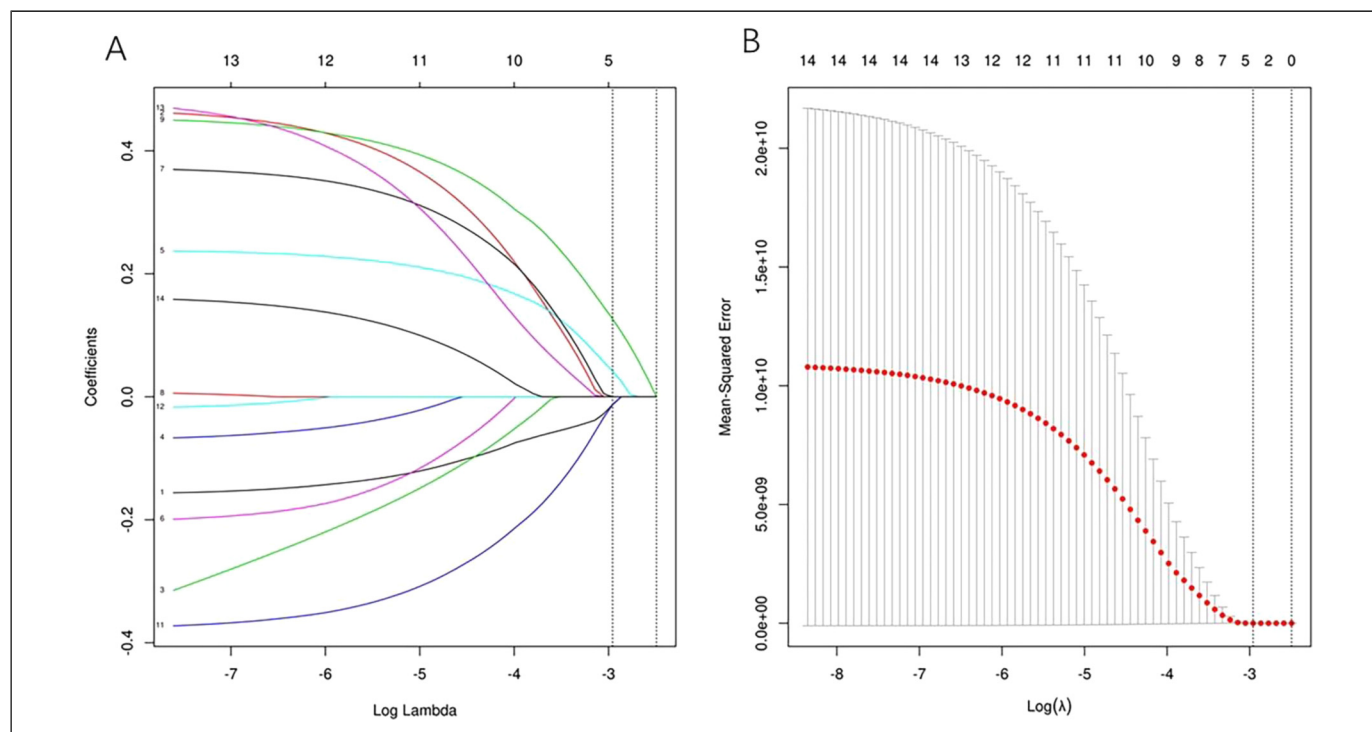


Figure 1. Radiomics feature selection with LASSO. After screening out the redundant features by LASSO, the 4 most robust radiomics features (including Least Axis Length, SDHGLE, median, and Skewness) were retained. The vertical line shows the value of λ , and the dashed lines on the left and right sides indicate the minimum standard and 1-standard error standard (1-SE). The predictive error of the minimum standard is very close to 1-SE. Sometimes, we tend to choose 1-SE to select a much more reduced model.

Abbreviations: LASSO, least absolute shrinkage and selection operator; SDHGLE, Small Dependence High Gray Level Emphasis.

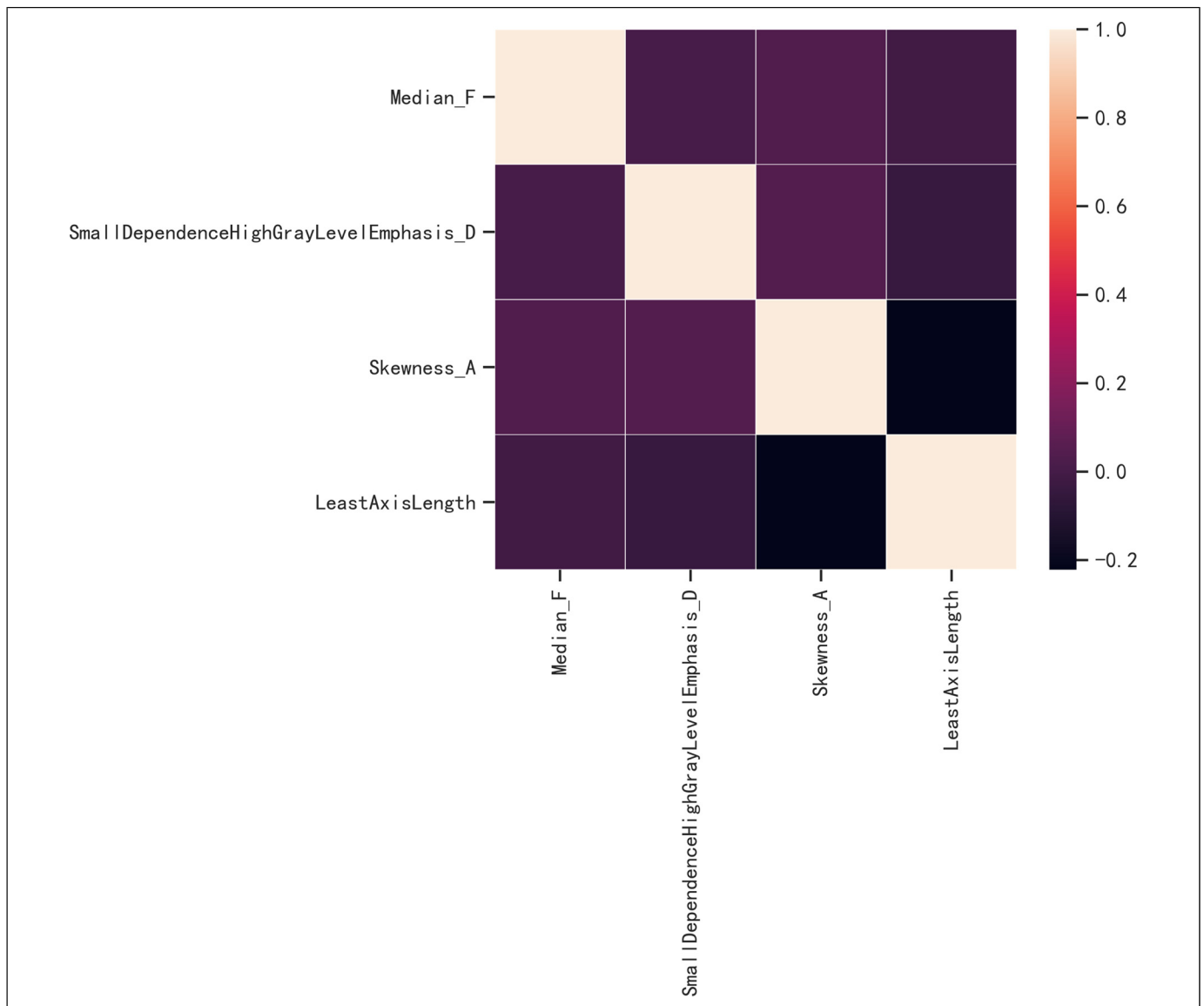


Figure 2. The correlation analysis of radiomic features. The correlation coefficient was between -0.222 and 0.041 . So there is no significant correlation between any 2 features. The correlation of characters in the model more than 0.6 will influence the stability of the model. Figure 2 shows that the correlation of the characters in the radiomics model was less than 0.6 . So it will not influence the stability of our model. A much clear Figure 2 has been provided in the article.

respectively, the 4 most robust radiomics features (Least Axis Length, Small Dependence High Gray Level Emphasis [SDHGLE], median, and skewness) were retained when the value of λ on the minimum standard. The relationship between the 4 radiomic features was significantly weak (Figures 1 and 2).

Machine learning models, including logistic regression (logistic), SVM, and decision tree, were developed based on the 4 radiomics features. The model established using the logistic method had the best performance, and the AUC values in the training and testing cohorts were 0.720 and 0.770 , respectively (Table 3 and Figure 3). The Radscore for each patient was then calculated using the selected features weighted by their respective coefficients in the logistic model, which can be expressed as follows: $\text{Radscore} = -0.026 + 0.410 \cdot \text{SDHGLE}$

$+ 0.222 \cdot \text{Skewness} - 0.245 \cdot \text{Median} - 0.223 \cdot \text{Least Axis Length}$. The Radscore for each patient in the training and testing cohorts is shown in Figure 4.

Combined Model Construction and Validation of Performance

Logistic regression was performed to establish a combined model based on the 5 clinical features and 4 radiomics features. And the nomogram was established (Supplemental Figure 3). The ROC-AUC of the combined model was 0.840 and 0.850 in the training and test groups, respectively (Table 3 and Figure 3). The Delong test revealed that the combined model

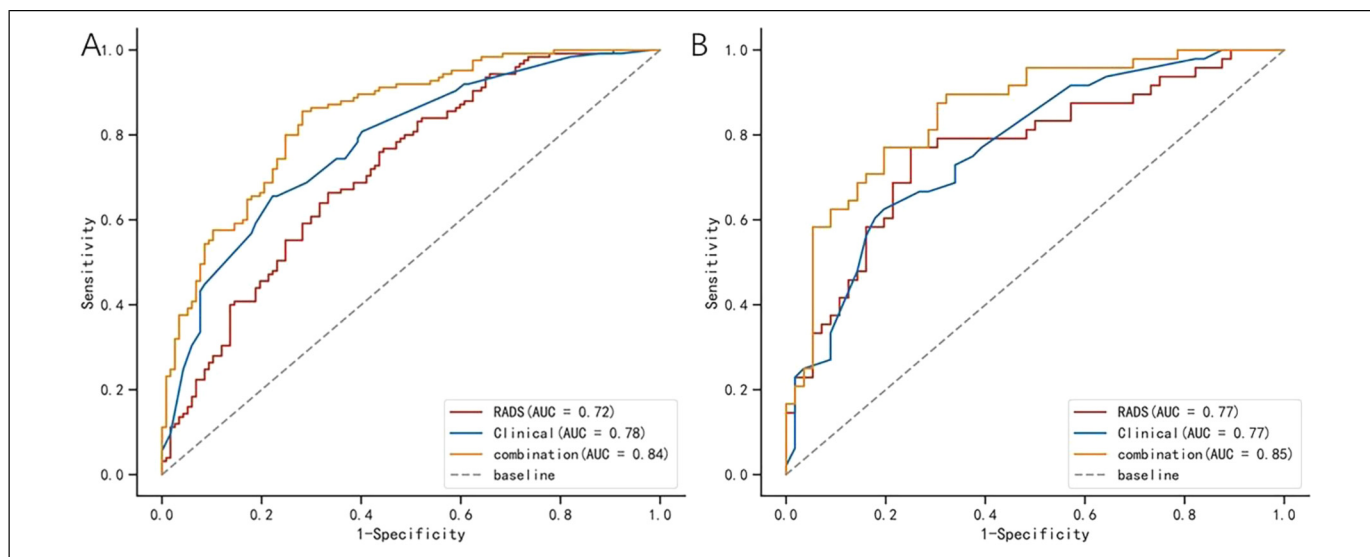


Figure 3. Comparison of ROC curves among the clinical model, radiomics model, and combined model respectively in the training cohorts (A) and testing cohorts (B). The AUC values in the combined model are better than in the clinical model and radiomics model for the prediction of IMA.

Abbreviations: ROC, receiver operating characteristic; AUC, area under the curve; IMA, invasive mucinous adenocarcinoma.

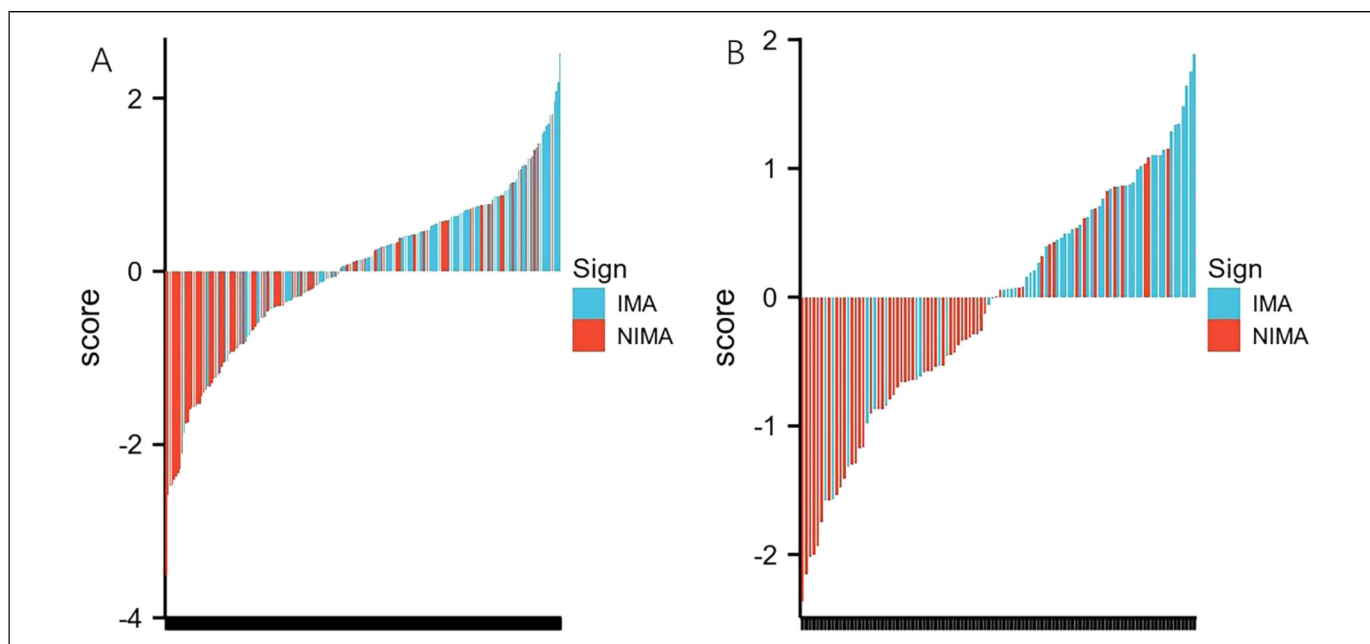


Figure 4. Bar charts of radscore for each patient in the training cohort (A) and testing cohort (B). The X-axis represents each patient, each bar represents one patient. Red bars indicate the Radscore for patients with NIMA, while blue bars indicate the Radscore for patients with IMA. Red bars above the zero-line or blue bars below the zero-line mean misclassification.

Abbreviations: IMA, invasive mucinous adenocarcinoma; NIMA, noninvasive mucinous adenocarcinoma;.

and radiomics model were superior to the clinical and radiomics models ($P = .018$ and $.020$, respectively). The DCA revealed that when the probability of the threshold was over 0%, the net benefits of the combined model for the prediction of IMA were higher than those of the clinical and radiomics models in both the training and testing cohorts. The Brier scores of the combined model were 0.161 and 0.154 in the training and

testing groups, respectively, and the calibration plots are shown in the figures (Supplemental Figures 1 and 2).

Discussion

In this study, we developed a model based on clinical and radiomic features to distinguish patients with IMA and non-IMA.

The results of this study revealed that when establishing clinical models, lesion location in the lower lobe, cystic cavity, pleural traction, ΔCT_V , and bronchial truncation play significant roles in distinguishing IMA from non-IMA. Similar results indicating that CT features, including lesion location in the lower lobe, cystic cavity, pleural traction, ΔCT_V , and bronchial truncation, are significantly related to IMA, have been reported.^{26–29} This difference may be attributed to the fact that the tumor cells of IMA originate from goblet or columnar epithelial cells. Relatively well-differentiated cancer cells can produce more mucus, which is affected by gravity. Therefore, it is often found in the lower lobe. Cysts appear in IMA because of incomplete obstruction of the bronchioles by mucus, resulting in alveolar hypoventilation. Contrarily, it may also be caused by internal necrosis of the tumor, which is discharged through the bronchus. The difference in the enhanced ΔCT_V between IMA and non-IMA may also result from the mucinous component within the mucinous adenocarcinoma. Alternatively, IMA with cancer cells with lower metabolic activity, which are mucin-rich tumor cells, may also result in lower ΔCT_V . The mucinous adenocarcinoma tumor cells spread diffuse along the walls of the bronchi and alveoli, secrete mucus, and block parts of the bronchi; nonetheless, mucinous adenocarcinoma tumor cells are less destructive to the bronchi than nonmucinous adenocarcinoma. Generally, nonmucinous adenocarcinomas tend to cause bronchial truncation less frequently than mucinous adenocarcinomas. Based on the clinical features, Cha et al³⁰ established a model to predict IMAs and the sensitivity and specificity of the model were 54.3% and 89.7%, respectively. Our study also developed a predictive model of IMA based on the characteristics above, and the ROC-AUC, sensitivity, and specificity of the model were

0.780 to 0.770, 65.6% to 62.5%, and 77.8% to 80.4% in the training and testing groups, respectively.

To explore a much more effective method for predicting IMA, we extracted 4 independent radiomic features associated with IMA: Skewness, Median, Small-Dependence High Gray Level Emphasis, and Least Axis Length. These parameters belong to the GLDM, histogram, and form factor parameters. Small Dependence High Gray Level Emphasis, one of the GLDM parameters, shows that the smaller the difference between the grayscale corresponding pixel and its adjacent pixels, the smaller the spatial change in the image, and the coarser the image texture. The Median, which is a histogram parameter, represents the median pixel value of an image (of the lesion). Another histogram feature was Skewness, which reflects the degree of asymmetry in the histogram distribution. If the predictive value was effective, the absolute values of the skewness would have been higher. The Least Axis Length is a form-factor parameter that is independent of the gray-level intensity distribution in the ROI. All the above features were the conversion of CT images into higher-throughput radiomics feature data. They allow high-throughput mining of quantitative imaging features from general medical images, followed by automated analysis to assist clinical decision-making. A previous study revealed that radiomic features were significantly related to the subtypes (adenocarcinoma and squamous cell carcinoma, small cell lung cancer, and nonsmall cell lung cancer) of lung cancer. Other studies have also revealed that radiomics features from CT could reflect the map of gene mutations in lung cancer, such as EGFR mutations, KRAS mutations, and PD-L1 expression. In this study, the model based on these radiomic features also demonstrated an effective role in predicting invasive mucinous adenocarcinomas. According to our ROC analyses, the

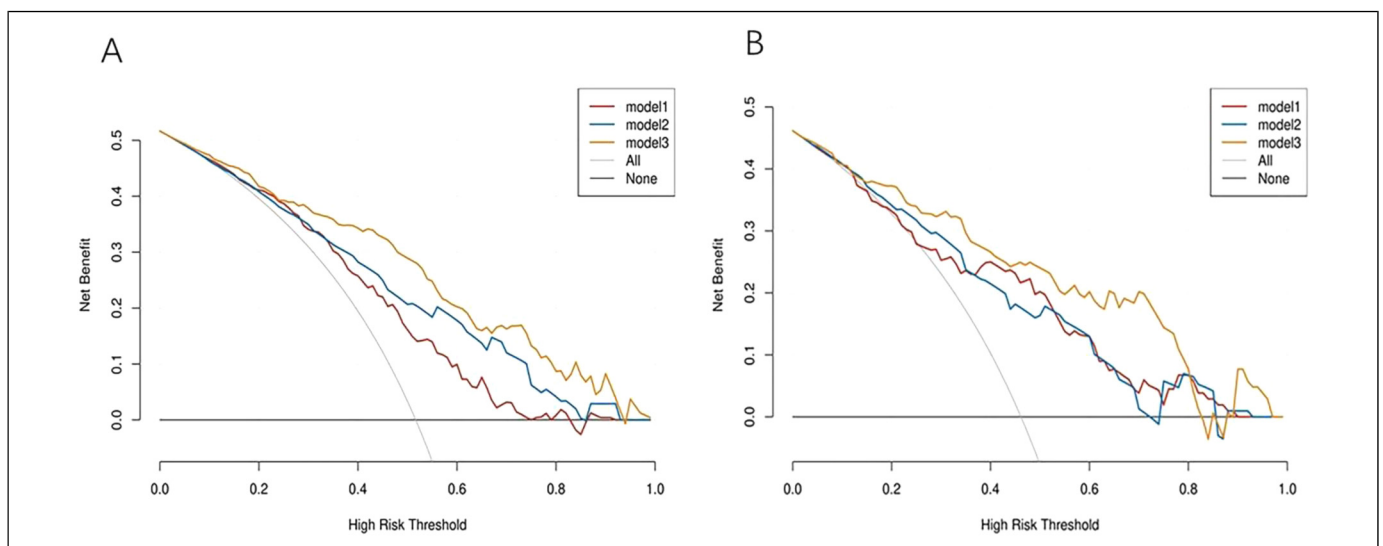


Figure 5. Decision curve analyses for the radiomics-clinical model compared with the radiomics model and clinical model in training cohort (A) and the testing cohort (B). The decision curve analysis presents that the net benefits of the combined model for the prediction of IMA were higher than the clinical model and radiomics model. Model 1 was the radiomics model, model 2 was the clinical model, and model 3 was the combined model. The decision curve analysis (DCA) showed that the line of the combined model was higher than the clinical model and the radiomics model when the probability ranged from 0 to 1.

AUC values for the radiomics model were 0.720 and 0.770 for the training and test groups, respectively. The clinical-radiomics combined model (ROC-AUC:0.840-0.850) was comparable for invasive mucinous adenocarcinoma, and it was significantly better than the clinical model. Furthermore, the decision curve analysis demonstrated that the combined model performed significantly better than the clinical and radiomic models in predicting outcomes. Decision curve analysis offers important information beyond the standard performance metrics of discrimination and calibration and could evaluate the clinical impact, indicating that they had a higher chance of success (Figure 5).

Although research bias was minimized through the propensity matching method, this study still has some limitations due to its retrospective nature. First, the sample size was relatively small, and only one institution participated in the study. Second, the CT images used in this study were acquired using different devices and scanning parameters, resulting in a potential bias in the analysis. But previous studies showed that the influences of these factors showed relatively consistent patterns.³¹ Third, owing to the short follow-up period after surgery, there was no predictive model for patient survival. To guide clinical practice, the model will be validated in a multicenter prospective manner in the future and will be further optimized.

In conclusion, in the present study, we established a model to predict IMA using clinicopathological, radiomic, and clinical-radiomic features for the first time. The clinical-radiomic model established by us also showed a good predictive value and has potential value in clinical practice. We will also conduct further studies to explore the tumor microenvironment for predicting tumor biological behavior in lung adenocarcinoma in the future to accurately evaluate the prognosis of patients and guide precision treatment.

Acknowledgments

None.

Authorship Statement

LG H and JJ Z performed the experiment and wrote the manuscript. M L and GF S delineated regions of interest (ROI) and extract the radiomics features. Q X was responsible for the design of the experiment.

Declaration of Conflicting Interests

The author(s) declared no potential conflicts of interest with respect to the research, authorship, and/or publication of this article.

Funding


The author(s) disclosed receipt of the following financial support for the research, authorship, and/or publication of this article: Key development plan of XingTai (ZC20301).

Ethics Statement

This study was performed following the Helsinki Declaration and approved by the Ethics Committee of our hospital (Ethics Committee of Hebei Medical University Fourth Affiliated Hospital,

reference number: 2022KS017, data 2022.6.27). Ethical approval was obtained from our hospital, and waivers of consent were granted to the study subjects.

ORCID iD

Ligang Hao  <https://orcid.org/0000-0003-2294-8778>

Supplemental Material

Supplemental material for this article is available online.

References

1. Sung H, Ferlay J, Siegel RL, et al. Global cancer statistics 2020: GLOBOCAN estimates of incidence and mortality worldwide for 36 cancers in 185 countries. *CA Cancer J Clin.* 2021;71(3):209-249. doi: 10.3322/caac.21660
2. Dong RF, Zhu ML, Liu MM, et al. EGFR mutation mediates resistance to EGFR tyrosine kinase inhibitors in NSCLC: from molecular mechanisms to clinical research. *Pharmacol Res.* 2021;167:105583. doi: 10.1016/j.phrs.2021.105583
3. Memmott RM, Wolfe AR, Carbone DP, Williams TM. Predictors of response, progression-free survival, and overall survival in patients with lung cancer treated with immune checkpoint inhibitors. *J Thorac Oncol.* 2021;16(7):1086-1098. doi: 10.1016/j.jtho.2021.03.017.
4. Travis WD, Brambilla E, Noguchi M, et al. International Association for the Study of Lung Cancer/American Thoracic Society/European Respiratory Society international multidisciplinary classification of lung adenocarcinoma. *J Thorac Oncol.* 2011;6(2):244-285. doi: 10.1097/JTO.0b013e318206a221
5. Travis WD, Brambilla E, Noguchi M, et al. International Association for the Study of Lung Cancer/American Thoracic Society/European Respiratory Society: international multidisciplinary classification of lung adenocarcinoma: executive summary. *Proc Am Thorac Soc.* 2011;8(5):381-385. doi: 10.1513/pats.201107-042ST.
6. Travis WD, Brambilla E, Nicholson AG, et al. The 2015 World Health Organization classification of lung tumors: impact of genetic, clinical and radiologic advances since the 2004 classification. *J Thorac Oncol.* 2015;10(9):1243-1260. doi: 10.1097/JTO.0000000000000630
7. Lee MA, Kang J, Lee HY, et al. Spread through air spaces (STAS) in invasive mucinous adenocarcinoma of the lung: incidence, prognostic impact, and prediction based on clinicoradiologic factors. *Thorac Cancer.* 2020;11(11):3145-3154. doi: 10.1111/1759-7714.13632
8. Lin G, Li H, Kuang J, et al. Acinar-predominant pattern correlates with poorer prognosis in invasive mucinous adenocarcinoma of the lung. *Am J Clin Pathol.* 2018;149(5):373-378. doi: 10.1093/ajcp/aqx170
9. Gow CH, Hsieh MS, Liu YN, Lee YH, Shih JY. Clinicopathological features and survival outcomes of primary pulmonary invasive mucinous adenocarcinoma. *Cancers (Basel).* 2021;13(16):652-662. doi: 10.3390/cancers13164103

10. Shang G, Jin Y, Zheng Q, et al. Histology and oncogenic driver alterations of lung adenocarcinoma in Chinese. *Am J Cancer Res.* 2019;9(6):1212-1223.
11. Cai L, Wang J, Yan J, et al. Genomic profiling and prognostic value analysis of genetic alterations in Chinese resected lung cancer with invasive mucinous adenocarcinoma. *Front Oncol.* 2020;10:603671. doi: 10.3389/fonc.2020.603671
12. Hu H, Pan Y, Li Y, et al. Oncogenic mutations are associated with histological subtypes but do not have an independent prognostic value in lung adenocarcinoma. *Onco Targets Ther.* 2014;7:1423-1437. doi: 10.2147/OTT.S58900
13. Boland JM, Maleszewski JJ, Wampfler JA, et al. Pulmonary invasive mucinous adenocarcinoma and mixed invasive mucinous/nonmucinous adenocarcinoma—a clinicopathological and molecular genetic study with survival analysis. *Hum Pathol.* 2018;71:8-19. doi: 10.1016/j.humpath.2017.08.002
14. Ichinokawa H, Ishii G, Nagai K, et al. Distinct clinicopathologic characteristics of lung mucinous adenocarcinoma with KRAS mutation. *Hum Pathol.* 2013;44(12):2636-2642. doi: 10.1016/j.humpath.2013.05.026.
15. Gow CH, Wu SG, Chang YL, Shih JY. Multidriver mutation analysis in pulmonary mucinous adenocarcinoma in Taiwan: identification of a rare CD74-NRG1 translocation case. *Med Oncol.* 2014;31(7):34. doi: 10.1007/s12032-014-0034-4
16. Hwang DH, Sholl LM, Rojas-Rudilla V, et al. KRAS and NKX2-1 mutations in invasive mucinous adenocarcinoma of the lung. *J Thorac Oncol.* 2016;11(4):496-503. doi: 10.1016/j.jtho.2016.01.010.
17. Ettinger DS, Wood DE, Aisner DL, et al. Non-Small Cell Lung Cancer, Version 5.2017, NCCN Clinical Practice Guidelines in Oncology. *J Natl Compr Canc Netw.* version 5.2017. 2017;15(4):504-535. doi: 10.6004/jnccn.2017.0050.
18. Aberle DR, Adams AM, Berg CD, et al. Reduced lung-cancer mortality with low-dose computed tomographic screening. *N Engl J Med.* 2011;365(5):395-409. doi: 10.1056/NEJMoa1102873
19. de Koning HJ, van der Aalst CM, de Jong PA, et al. Reduced lung-cancer mortality with volume CT screening in a randomized trial. *N Engl J Med.* 2020;382(6):503-513. doi: 10.1056/NEJMoa1911793
20. Aerts HJ, Velazquez ER, Leijenaar RT, et al. Decoding tumour phenotype by noninvasive imaging using a quantitative radiomics approach. *Nat Commun.* 2014;5:4006. doi: 10.1038/ncomms5006
21. Vicini S, Bortolotto C, Rengo M, et al. A narrative review on current imaging applications of artificial intelligence and radiomics in oncology: focus on the three most common cancers. *Radiol Med.* 2022;127(8):819-836. doi: 10.1007/s11547-022-01512-6
22. Ardila D, Kiraly AP, Bharadwaj S, et al. End-to-end lung cancer screening with three-dimensional deep learning on low-dose chest computed tomography. *Nat Med.* 2019;25(6):954-961. doi: 10.1038/s41591-019-0447-x
23. Zhang K, Liu X, Shen J, et al. Clinically applicable AI system for accurate diagnosis, quantitative measurements, and prognosis of COVID-19 pneumonia using computed tomography. *Cell.* 2020;182(5):1360. doi: 10.1016/j.cell.2020.08.029
24. Tian P, He B, Mu W, et al. Assessing PD-L1 expression in non-small cell lung cancer and predicting responses to immune checkpoint inhibitors using deep learning on computed tomography images. *Theranostics.* 2021;11(5):2098-2107. doi: 10.7150/thno.48027
25. van Griethuysen JJM, Fedorov A, Parmar C, et al. Computational radiomics system to decode the radiographic phenotype. *Cancer Res.* 2017;77(21):e104-e107. doi: 10.1158/0008-5472.CAN-17-0339
26. Xu L, Li C, Lu H. Invasive mucinous adenocarcinoma of the lung. *Transl Cancer Res.* 2019;8(8):2924-2932. doi: 10.21037/tcr.2019.11.02.
27. Jie B, Yinhuo J, Qifeng H, et al. Analysis of MSCT findings in primary pulmonary mucinous adenocarcinoma with pathology. *J Med Imaging.* 2020;30(5):871-874.
28. Yuanwei S, Minmin T, Xiaolei W, et al. Clinicopathological features and CT findings of primary pulmonary invasive mucinous adenocarcinoma. *J Chin Clin Med Imaging.* 2020;31(10):719-722,726.
29. Qingyi W, Wanhu L, Dexian Z, et al. Imaging findings and pathological features of primary lung invasive mucinous adenocarcinoma. *Chin J Cancer Prev Treat.* 2020;27(8):647-652,657.
30. Cha MJ, Lee KS, Kim TJ, et al. Solitary nodular invasive mucinous adenocarcinoma of the lung: imaging diagnosis using the morphologic-metabolic dissociation sign. *Korean J Radiol.* 2019;20(3):513-521. doi: 10.3348/kjr.2018.0409
31. Peng X, Yang S, Zhou L, et al. Repeatability and reproducibility of computed tomography radiomics for pulmonary nodules: a multicenter phantom study. *Invest Radiol.* 2022;57(4):242-253. doi: 10.1097/RLI.0000000000000834